Materials Horizons

COMMUNICATION

View Article Online
View Journal | View Issue

Check for updates

Cite this: *Mater. Horiz.*, 2020, 7, 592

Received 13th August 2019,
Accepted 31st October 2019

DOI: 10.1039/c9mh01261c

rsc.li/materials-horizons

Published on 31 octubre 2019. Downloaded on 31/7/2024 01:20:01.

High-κ polymers of intrinsic microporosity: a new class of high temperature and low loss dielectrics for printed electronics†

Zhongbo Zhang, ‡[a] Jifu Zheng, ‡[b] Kasun Premasiri, ‡[c] Man-Hin Kwok,[a] Qiong Li,[a] Ruipeng Li,[d] Suobo Zhang,[b] Morton H. Litt,[a] Xuan P. A. Gao[c] and Lei Zhu *[a]

High performance polymer dielectrics are a key component for printed electronics. In this work, organo-soluble polymers of intrinsic microporosity (PIMs) are reported for the first time to demonstrate desirable dielectric properties with a high permittivity (or κ), heat resistance, and low dielectric loss simultaneously. Due to the highly dipolar sulfonyl side groups (4.5 D) and rigid contorted polymer backbone, a sulfonylated PIM (SO_2-PIM) enabled friction-free rotation of sulfonyl dipoles in the nanopores. As such, an optimal balance between relatively high κ and low dielectric loss is achieved in a broad temperature window (−50–200 °C). For example, the discharged energy density reached 17 J cm^{-3} with κ = 6.0. The discharge efficiency was 94% at 150 °C/300 MV m^{-1} and 88% at 200 °C/200 MV m^{-1}. Furthermore, its application as a high-κ gate dielectric in field effect transistors (FETs) is demonstrated. With the bilayer SO_2-PIM/SiO_2 gate dielectric, InSe FETs exhibited a high electron mobility in the range of 200–400 cm^2 V^{-1} s^{-1}, as compared to 40 cm^2 V^{-1} s^{-1} for the bare SiO_2-gated InSe FET. This study indicates that highly dipolar PIMs with a rigid polymer backbone and large free volume are promising as next generation gate dielectric materials for printed electronics.

New concepts

In this work, a new concept of a friction-free dipolar glass polymer is demonstrated using novel sulfonylated polymers of intrinsic microporosity (SO_2-PIMs). First, the nanopores in PIMs provide large free volume for friction-free rotation of side-chain dipolar groups. Second, the sulfonyl group has a large dipole moment of 4.5 D to promote orientational polarization. Third, the rigid, contorted, ladder-like backbone of PIM enables a high glass transition temperature (T_g, above the thermal degradation temperature). As a result of friction-free rotation of sulfonyl dipoles in the nanopores below the T_g, SO_2-PIM shows a dissipation factor as low as 0.005, while achieving a high dielectric constant (κ = 6) and a high discharged energy density of 17 J cm^{-3} with discharge efficiency >90% at room temperature. Even at 175 °C, the discharge efficiency maintained at 86%, indicating excellent heat tolerance. Compared to existing high κ dipolar polymers, this concept has never been demonstrated before. Furthermore, the dielectric performance of SO_2-PIM is tested in the InSe field-effect transistors (FETs). Intriguingly, the high κ SO_2-PIM significantly promotes the electron mobility in InSe to 200–400 cm^2 V^{-1} s^{-1}. This work demonstrates that SO_2-PIMs are promising as next generation gate dielectric materials for printed electronics.

High-dielectric constant (or high-κ) and low-loss polymer dielectrics are highly desirable for power and electronic applications, including electric energy storage[1–3] and printed electronics[4,5] such as in human performance monitoring,[6] information storage devices,[7] and soft robotics.[8] One important component for all hybrid electronic devices is the organic field effect transistor (FET), where high-κ/low-loss gate dielectrics play an important role.[9–12] The state-of-the-art gate dielectric used in industry is self-assembled monolayer (SAMs, ∼2 nm) passivated silica (SiO_2) or silicon oxynitride, which can induce high hole mobility (μ_h) for semiconductors.[13] However, SiO_2 has a relatively low κ of 3.9, and the leakage current increases exponentially as its thickness decreases to below 50 nm due to Fowler–Nordheim electron tunneling.[14,15] It has been a challenge to search for high-κ/low-loss printable dielectrics that can fulfill the stringent requirements for organic FETs, including but not limited to, κ > 5–10, capacitance >20 nF cm^{-2}, low leakage, high breakdown strength, and long lifetime.

Theoretically, the capacitance density (C_g, in F m^{-2}) of a gate dielectric is defined as: $C_g = \varepsilon_0(\kappa/d)$, where ε_0 is vacuum permittivity and d is thickness of the effective layer. Fundamentally, there are two ways to achieve high capacitance density: decreasing d and/or increasing κ. In the past three decades,

[a] *Department of Macromolecular Science and Engineering, Case Western Reserve University, 2100 Adelbert Road, 44106-7202, USA. E-mail: lxz121@case.edu*
[b] *Key Laboratory of Ecomaterials, Changchun Institute of Applied Chemistry, Chinese Academy of Sciences, Changchun 130022, P. R. China*
[c] *Department of Physics, Case Western Reserve University, 2076 Adelbert Road, Cleveland, Ohio 44106, USA*
[d] *National Synchrotron Light Source II, Brookhaven National Laboratory, Upton, New York 11973, USA*

† Electronic supplementary information (ESI) available. See DOI: 10.1039/c9mh01261c

‡ These authors contributed equally to this work and should be considered as co-first authors.

This journal is © The Royal Society of Chemistry 2020

Published on 31 octubre 2019. Downloaded on 31/7/2024 01:20:01.

research has been focused on decreasing d, rather than increasing κ, because it has been difficult to increase κ above 5 for linear dielectric polymers.[1,16] For example, neat SAMs (2–4 nm thick) and ultrathin polymer films (15–20 nm) have been reported to show a high capacitance density, *i.e.*, >300 nF cm^{-2}.[13] However, manufacturing defects in SAMs, as well as ultrathin polymer films, limits the device size to 0.1 mm^2 (*e.g.*, both molecular and mesoscale pinholes and grain boundaries are present in SAMs[17]), despite decades of research to push for molecularly thin dielectrics.[18] Grand challenges exist to achieving defect-free molecular dielectrics using currently available manufacturing processes.[18]

Given the recent advances,[1,2] an alternative approach to achieving high performance organic FETs is to increase the permittivity of the polymer dielectric above 5–10 while keeping low dielectric loss. In this way, relatively thick polymer films (0.3–1.0 μm) can be printed or spin-coated, which will decrease the pinhole density while a high C_g can still be obtained *via* the high κ gate dielectric. The first attempt is to utilize high κ poly(vinylidene fluoride-*co*-trifluoroethylene) [P(VDF-TrFE)]-based random copolymers and terpolymers (κ = 50–70).[19] These high κ fluoropolymers have been applied for organic FETs.[20,21] However, a high dissipation factor ($\tan\delta$) of $\geq$0.02 is observed, and the applicable frequency is limited at $<10^4$ Hz due to the slow switching of ferroelectric domains.

The second strategy is to utilize the space charge polarization (*i.e.*, conduction of ions). Based on the electric double layer (EDL) theory,[22] the capacitance from EDL can be at least 1000 times that of the dipolar capacitance of bulk polymers. Recently, ion gel gate dielectrics have been developed, which exhibit ultrahigh capacitance density, around 3–100 μF cm^{-2} at 1 Hz.[23] However, the operation frequency is limited at $<10^4$ Hz due to slow ion motion. The $\tan\delta$ is around 0.09–0.20 for EDL capacitors,[23] too high for many practical FET applications.

Recently, dipolar glass (DG) polymers have attracted substantial attention because of their high κ and low loss below the glass transition temperaure (T_g). Basically, DG polymers utilize the sub-T_g transitions to enhance orientational polarization.[1,24] Most of these DG polymers contain cyanoethyl side groups (3.9 D).[25–27] For example, Shin-Etsu Chemical commercialized cyanoethylated pullulan (CEP, ~90% functionality). Because of the relatively rigid cellulose backbone, the T_g reached ~110 °C,[28] and the room temperature permittivity was ~16 at frequencies below 10^4 Hz.[29] However, CEP suffers from relativley high loss ($\tan\delta > 0.02$) and low breakdown strength (~80 MV m^{-1}).

Highly dipolar sulfonyl side groups are also used in DG polymers because of the high dipole moment of 4.5 D. Different from main-chain sulfonyl polymers,[30,31] sulfonylated side chain polymers are more advantageous to enhance the dielectric constant because of the high mobility of side chain dipoles. For example, sulfonyl-containing polymethacrylates[32,33] and polyethers[34] exhibited high κ values between 7 and 12. However, they again suffer from relatively low T_g (<125 °C). Most recently, sulfonylated poly(2,6-dimethyl-1,4-phenylene oxide)s (SO_2-PPOs) with a rigid polymer backbone and high T_g above

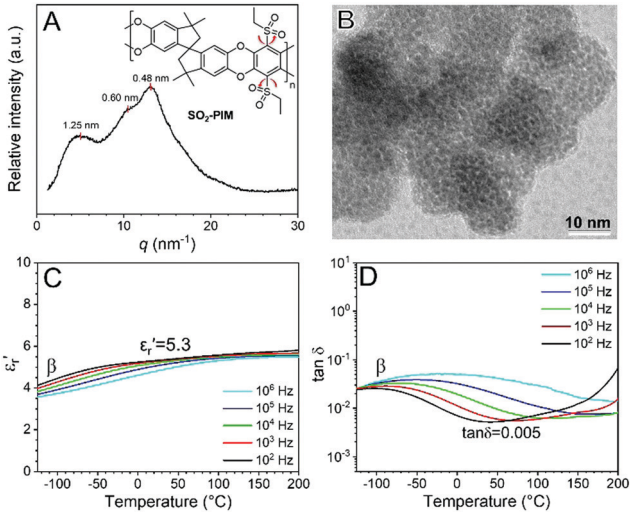

Fig. 1 (A) One-dimensional WAXD profile for the as-cast SO_2-PIM (the chemical structure is in the inset). (B) Bright-field TEM micrograph of SO_2-PIM stained by RuO_4 for 10 min. Temperature-scan BDS results of (C) the real part of the relative permittivity (ε_r') and (D) $\tan\delta$ at different frequencies.

200 °C was reported.[35] They demonstrated a high κ of 6–8, a relatively low dielectric loss, and heat resistence up to 150 °C.

In this work, we report for the first time that polymers of intrinsic microporosity (PIMs) can be used as a new class of DG polymers for high-performance FETs. With a large free volume, rigid and contorted ladder-like backbones, and high T_g (above the thermal degradation temperature), high-κ and low-loss PIMs are realized by attaching dipolar sulfonyl groups to the backbone of an organosoluble PIM (SO_2-PIM, see the inset in Fig. 1A).[36] This could be attributed to the friction-free rotation of sulfonyl dipoles in the nanopores. A high κ of 5–6 was obtained and the discharged energy density (U_e) was as high as ~17 J cm^{-3} with the dissipation loss as low as $\tan\delta \sim 0.005$. More importantly, the SO_2-PIM exhibited a high discharge efficiency of 94% at 150 °C and 300 MV m^{-1}, demonstrating the outstanding heat resistance. Finally, its application as a high-κ gate dielectric in the InSe FETs was verified, and an enhanced electron mobility of 200–400 cm^2 V^{-1} s^{-1} was achieved.

Scheme S1 in the ESI† shows the modified synthesis of SO_2-PIM. It was reported that high monomer concentration (>25%) and high temperature (160 °C) led to a high molecular weight for PIM-1, because a short reaction time could prevent crosslinking.[36] However, the Ar–$SO_2CH_2CH_3$ group was too acidic because of strong electron withdrawing ability of the sulfonyl group, and it could react readily with the base (K_2CO_3) to generate a crosslinked structure (Scheme S2, ESI†). To avoid crosslinking, the disulfinyl monomer was used for the condensation polymerization instead of the disulfonyl monomer, because the electron withdrawing ability of the sulfinyl group is weaker. The condensation polymerization was stopped after 80 min at 160 °C, and no crosslinking was observed. Then, the obtained SO-PIM was fully oxidized using *m*-chloroperbenzoic acid (*m*-CPBA) in chloroform to afford SO_2-PIM. After slow precipitation in acetone, low molecular weight fractions were removed.

Published on 31 octubre 2019. Downloaded on 31/7/2024 01:20:01.

The molecular weight and molecular weight distribution of the purified polymer were determined by size-exclusion chromatography (SEC) using *N*,*N*-dimethylformamide (DMF) as a solvent and polystyrene as a standard. The number-average molecular weight (M_n) was 360 000 Da and the molecular weight distribution was 3.3. The SO_2-PIM was soluble in various organic solvents such as chloroform, tetrahydrofuran, DMF, *N*,*N*-dimethylacetamide (DMAc), and dimethylsulfoxide (DMSO). Using this revised synthetic method, high quality SO_2-PIM films could be obtained by solution-casting for dielectric measurements. Proton nuclear magnetic resonance and SEC characterization results are presented in Fig. S1–S3 (ESI†).

Films of SO_2-PIM (25–30 μm) were obtained by solution-casting from chloroform. Wide-angle X-ray Diffraction (WAXD) showed multiple broad peaks, corresponding to different pore sizes (0.5–1.25 nm) (Fig. 1A). The pore morphology was studied by transmission electron microscopy (TEM); see Fig. 1B. The SO_2-PIM was stained by RuO_4 vapor for 10 min. Since RuO_4 preferentially stained aromatic rings, the polymer struts appeared dark and the pores appeared brighter. From the TEM projection image, the average pore width was *ca.* 0.6 nm with a run length of 1.2–1.5 nm, which fit with the WAXD result well. These nanopores provided large free volume for friction-free rotation of the sulfonyl dipoles. The linear dielectric property was studied by conventional broadband dielectric spectroscopy (BDS). In Fig. 1C, the dielectric constant (*i.e.*, the real part of relative permittivity, ε_r') at 1 kHz increased from 4.0 at −125 °C to 5.3 at room temperature, owing to the orientational polarization of two ethylsulfonyl side groups. The dipolar relaxation could be clearly seen in $\tan\delta$ (Fig. 1D) and the ε_r'' (*i.e.*, the imaginary part of relative permittivity, Fig. S4, ESI†). The sub-T_g (*i.e.*, β) transition took place around −75 °C at 1 kHz, and was assigned to the rotation of ethylsulfonyl side groups in the free volume. The frequency-scan BDS results for SO_2-PIM at different temperatures are shown in Fig. S5 (ESI†). The peak β transition could be observed at high frequencies, *i.e.*, $> 10^6$ Hz, when the temperature was above 50 °C. Meanwhile, the lowest $\tan\delta$ reached as low as 0.005 for the SO_2-PIM around 40 °C and 1 kHz. This was a result of the high T_g and thus largely frozen chain dynamics. The high-field dielectric behavior of SO_2-PIM was further studied using high voltage BDS (HV-BDS).[37] In Fig. S6 (ESI†), all $\tan\delta$ curves under different electric fields largely overlapped, except for slightly enhanced conduction of impurity ions above 50 °C. This result indicated that no significant dielectric nonlinearity was observed up to 71.4 MV m^{-1}. This was different from main-chain dipolar glass polymers reported recently,[37] where significant dielectric loss was observed as a result of high field-induced cooperative segmental motions.

The high-field dielectric property was studied by unipolar *D*–*E* loop measurements, and discharged U_e and efficiency were obtained from the charge and discharge curves (Fig. 2). At 1 kHz, extremely narrow loops were obtained below 450 MV m^{-1} (Fig. 2A) with a discharge efficiency above 97% (Fig. 2B), indicating that the sulfonyl dipoles were isolated and did not form any ferroelectric domains under the high poling field.

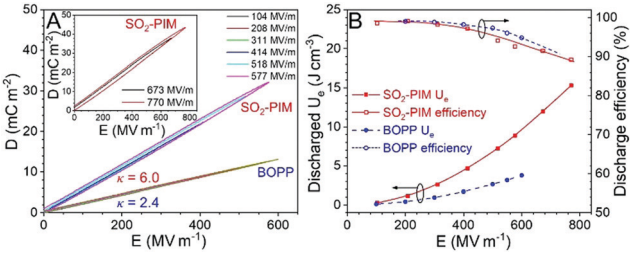

Fig. 2 (A) Unipolar *D*–*E* loops for SO_2-PIM under 1 kHz at room temperature. (B) Discharged energy density (U_e) and discharge efficiencies as a function of the poling field for SO_2-PIM. BOPP is used for comparison.

This is different from low-T_g (<125 °C) sulfone-containing dipolar glass polymers,[34] where weak ferroelectric domains could still form under a high enough electric field (>400 MV m^{-1}). A high κ of 6.0 was obtained from the slope of the linear loops.

Compared with the state-of-the-art BOPP film, the discharge efficiency was similar; however, the discharged U_e of SO_2-PIM was about 2.5 times that of BOPP. When the poling field increased to above 500 MV m^{-1}, dielectric loss became more pronounced (Fig. 2A), which could be attributed to enhanced electronic conduction under high electric fields.[38] However, the discharge efficiency was still ≥90% (Fig. 2B). When the poling field reached 770 MV m^{-1}, a high discharged U_e of 17 J cm^{-3} was achieved.

Similar to other reports,[36] no glass transition was found for SO_2-PIM before the onset of thermal degradation (*i.e.*, 360 °C with 1 wt% weight loss). The exceptionally high T_g of PIMs is desired for high-temperature dielectric applications. Fig. 3A shows high temperature bipolar *D*–*E* loops for the SO_2-PIM film polarized at 300 MV m^{-1} (1 kHz). Below 150 °C, slim loops were observed. Fig. 3B presents the discharged U_e and discharge efficiency for SO_2-PIM as a function of temperature, and the recently reported SO_2-PPO_{25} was used for comparison.[35] At 100 °C, SO_2-PPO_{25} exhibited a higher discharged U_e than SO_2-PIM because of its higher κ of 6.2. However, SO_2-PIM had a higher discharge efficiency (94.4%) than that of SO_2-PPO_{25} (91%). Upon increasing the temperature to 150 °C, the discharged U_e of SO_2-PIM remained nearly constant and the discharge efficiency only slightly decreased to 93%. However, both the discharged U_e and discharge efficiency of SO_2-PPO_{25} significantly decreased upon increasing the temperature to 150 °C. This was explained by enhanced charge injection from electrodes and thus high electronic conduction at elevated temperatures.[35] Considering similar dielectric constants, it should be the higher T_g and suppressed space charge injection from metal electrodes for SO_2-PIM to exhibit a lower dielectric loss than SO_2-PPO_{25}. Even at 175 °C, the SO_2-PIM film still exhibited a reasonable discharge efficiency of 86%. When the poling field decreased to 200 MV m^{-1}, high discharge efficiencies were still observed, *i.e.*, 94% at 175 °C and 88% at 200 °C (Fig. 3C). These high temperature discharge efficiencies were comparable to a crossliniked divinyltetramethyldisiloxanebis-(benzocyclo-butene)/boron nitride nanosheet (c-BCB/BNNS) composite reported recently.[39] However, the discharged U_e of SO_2-PIM

 This journal is © The Royal Society of Chemistry 2020

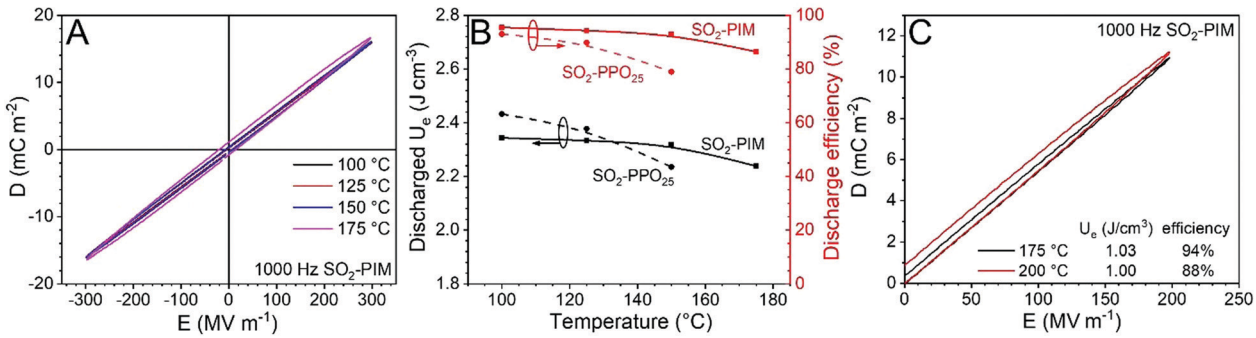

Fig. 3 (A) Bipolar D–E loops at high temperatures for SO_2-PIM. (B) Tempearture-dependent discharged energy density (U_e) and discharge efficiency for SO_2-PIM and SO_2-PPO under 300 MV m^{-1}. (C) Unipolar D–E loops under 200 MV m^{-1} for SO_2-PIM at 175 and 200 °C, respectively.

Published on 31 octubre 2019. Downloaded on 31/7/2024 01:20:01.

was about twice that of c-BCB/BNNS because of its higher dielectric constant, *i.e.*, 6.0 for SO_2-PIM *vs.* 3.1 for c-BCB/BNNS.

Finally, the SO_2-PIM was applied as a high-κ gate dielectric for InSe-based FETs. InSe is a 2D semiconductor with high electron mobility as well as strong spin–orbit coupling and has drawn a lot of attention in the past few years for the fabrication of high performance 2D semiconductor FETs or transport devices.[40–42] As shown in Fig. 4A, an InSe nanoflake (~20 nm thick) was exfoliated onto a Si/SiO_2 substrate coated with SO_2-PIM where both the silicon oxide (300 nm) and SO_2-PIM (300–800 nm) were used as the gate dielectric. Electron beam evaporation was used to deposit a 5 nm layer of Ti followed by a 40 nm layer of Ni to form the source and drain electrodes contacting the InSe nanoflake on the SO_2-PIM layer. The degenerately doped n-type Si substrate was used as the back-gate electrode. The InSe channel length was about 20 μm. To ensure good insulation, the leakage current density (J) was tested for a solution-cast SO_2-PIM thin film capacitor (205 nm)

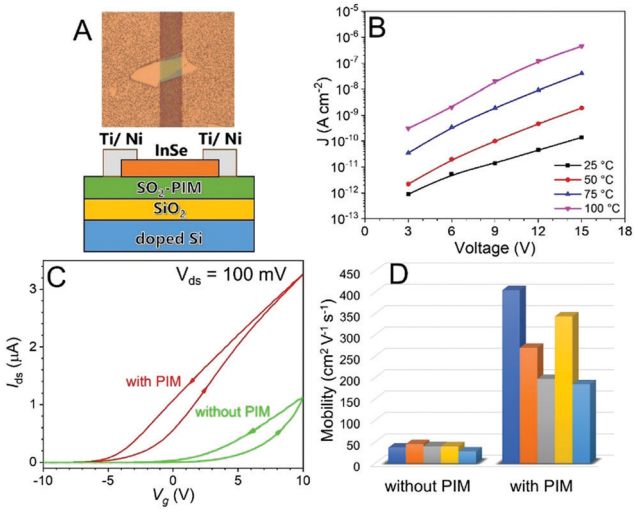

Fig. 4 (A) Schematic of the InSe-based FET device and the top-view optical microscopy image. (B) Leakage current density as a function of voltage in a capacitor device. (C) The I_{ds}–V_g transfer curve and (D) comparison of electron mobility in InSe for the FET devices with and without SO_2-PIM. Five devices were tested for each type of FET.

at different temperatures. As seen in Fig. 4B, low J values of 8.8×10^{-13} A cm^{-2} at 3 V and 1.4×10^{-10} A cm^{-2} at 15 V were observed for SO_2-PIM at room temperature. At 100 °C, the insulating property of SO_2-PIM was still preserved with a relativley low J value of 1.9×10^{-9} A cm^{-2} at 6 V.

Typical I_{ds}–V_g transfer curves are shown in Fig. 4C for the FET devices with and without SO_2-PIM. The electron's field effect mobility could be calculated from the linear region of the transfer curves. Note that the hysteresis in the transfer curves could be attributed to certain surface defects on the dielectric layer that allowed certain charge injection.[43] All FET devices with SO_2-PIM exhibited a high electron mobility between 180 and 400 cm^2 V^{-1} s^{-1}, about 10× higher than those for the FET devices without SO_2-PIM (Fig. 4D). The enhancement of mobility could be attributed to the screening effect from high-κ polar polymers.[40,44] Namely, the SO_2-PIM layer was used for screening interfacial Coulomb impurities, such as hydroxyl groups, moisture, and other chemical absorptions, resulting in improved charge carrier mobility and better performance of InSe FETs. Furthermore, I_{ds}–V_g transfer curves in the logarithmic scale and I_{ds}–V_{ds} curves are shown in Fig. S7 (ESI†), demonstrating more clearly the ON–OFF switching of the device and ohmic behavior of the contacts. It can be seen in Fig. S7 (ESI†) that there was an indication of improved ON–OFF ratio with the presence of the SO_2-PIM dielectric in the InSe FET, and the ON–OFF ratio reached at least 10^4 with the SO_2-PIM gate dielectric (the actual ON–OFF ratio should be higher than 10^4 shown in Fig. S7 (ESI†), since the true OFF state was not reached in the measurement due to the limited sensitivity of the instrument). Combining relatively high dielectric constant, low dielectric loss, low leakage, and high-temperature tolerance, dipolar SO_2-PIM is promising as a polymer gate dielectric for high-performance FETs.

In summary, utilizing highly polarizable sulfonyl groups, we introduced a new class of high-κ (5.3–6.0), high temperature (up to 200 °C), and low loss ($\tan\delta \sim 0.005$) dielectric, SO_2-PIM. The large pores (0.5–1.25 nm) were beneficial for the friction-free rotation of sulfonyl side groups. The highly rigid polymer structure with a high T_g prevented the backbone motions, resulting in low leakage current, high breakdown strength, and low dielectric loss at high temperatures. At room temperature,

the discharged U_e reached 17 J cm^{-3} at 770 MV m^{-1}. When it was used as a high-κ gate dielectric in the InSe FET device, a high electron mobility of 180–400 cm^2 V^{-1} s^{-1} was achieved. These experimental results demonstrated exciting prospects for the polar PIMs to be used as high-performance dielectrics in printed electronics.

Conflicts of interest

The authors declare no competing financial interests.

Acknowledgements

This work is supported by the National Science Foundation, Division of Materials Research, Polymers (DMR-1708990) and Condensed Matter Physics (DMR-1607631) Programs. This research used the 11-BM CMS beamline of National Synchrotron Light Source-II, Brookhaven National Laboratory (BNL), a U.S. Department of Energy User Facility operated for the Office of Science under contract No. DE-SC0012704.

Published on 31 octubre 2019. Downloaded on 31/7/2024 01:20:01.

References

1 L. Zhu, *J. Phys. Chem. Lett.*, 2014, **5**, 3677–3687.
2 Prateek, V. K. Thakur and R. K. Gupta, *Chem. Rev.*, 2016, **116**, 4260–4317.
3 E. Baer and L. Zhu, *Macromolecules*, 2017, **50**, 2239–2256.
4 G. Wang, N. Persson, P. H. Chu, N. Kleinhenz, B. Y. Fu, M. Chang, N. Deb, Y. M. Mao, H. Z. Wang, M. A. Grover and E. Reichmanis, *ACS Nano*, 2015, **9**, 8220–8230.
5 G. Wang, W. Huang, N. D. Eastham, S. Fabiano, E. F. Manley, L. Zeng, B. H. Wang, X. A. Zhang, Z. H. Chen, R. Li, R. P. H. Chang, L. X. Chen, M. J. Bedzyk, F. S. Melkonyan, A. Facchetti and T. J. Marks, *Proc. Natl. Acad. Sci. U. S. A.*, 2017, **114**, E10066–E10073.
6 Y. Khan, A. E. Ostfeld, C. M. Lochner, A. Pierre and A. C. Arias, *Adv. Mater.*, 2016, **28**, 4373–4395.
7 S. T. Han, Y. Zhou and V. A. L. Roy, *Adv. Mater.*, 2013, **25**, 5425–5449.
8 F. Carpi, D. De Rossi, R. Kornbluh, R. E. Pelrine and P. Sommer-Larsen, *Dielectric Elastomers as Electromechanical Transducers: Fundamentals, Materials, Devices, Models and Applications of an Emerging Electroactive Polymer Technology*, Elsevier, Oxford, UK, 2008.
9 A. Facchetti, M. H. Yoon and T. J. Marks, *Adv. Mater.*, 2005, **17**, 1705–1725.
10 Y. G. Ha, K. Everaerts, M. C. Hersam and T. J. Marks, *Acc. Chem. Res.*, 2014, **47**, 1019–1028.
11 R. P. Ortiz, A. Facchetti and T. J. Marks, *Chem. Rev.*, 2010, **110**, 205–239.
12 Y. H. Chou, H. C. Chang, C. L. Liu and W. C. Chen, *Polym. Chem.*, 2015, **6**, 341–352.
13 S. A. DiBenedetto, A. Facchetti, M. A. Ratner and T. J. Marks, *Adv. Mater.*, 2009, **21**, 1407–1433.
14 A. A. Demkov and A. Navrotsky, *Materials Fundamentals of Gate Dielectrics*, Springer, Dordrecht, Netherland, 2005.
15 A. Gupta, P. Fang, M. Song, M. R. Lin, D. Wollesen, K. Chen and C. M. Hu, *IEEE Electron Device Lett.*, 1997, **18**, 580–582.
16 Q. Chen, Y. Shen, S. Zhang and Q. M. Zhang, *Annu. Rev. Mater. Res.*, 2015, **45**, 433–458.
17 C. Vericat, M. E. Vela, G. Benitez, P. Carro and R. C. Salvarezza, *Chem. Soc. Rev.*, 2010, **39**, 1805–1834.
18 R. L. McCreery and A. J. Bergren, *Adv. Mater.*, 2009, **21**, 4303–4322.
19 L. Yang, X. Li, E. Allahyarov, P. L. Taylor, Q. M. Zhang and L. Zhu, *Polymer*, 2013, **54**, 1709–1728.
20 J. H. Li, Z. H. Sun and F. Yan, *Adv. Mater.*, 2012, **24**, 88–93.
21 X. Chen, L. Liu, S. Z. Liu, Y. S. Cui, X. Z. Chen, H. X. Ge and Q. D. Shen, *Appl. Phys. Lett.*, 2013, **102**, 063103.
22 J. O. M. Bockris, A. K. N. Reddy and M. Gamboa-Aldeco, *Modern Electrochemistry 2A*, Kluwer Academic Publishers, New York, 2nd edn, ch. 6, 2000.
23 S. H. Kim, K. Hong, W. Xie, K. H. Lee, S. Zhang, T. P. Lodge and C. D. Frisbie, *Adv. Mater.*, 2013, **25**, 1822–1846.
24 J. R. Fried, in *Physical Properties of Polymers Handbook*, ed. J. E. Mark, Springer, New York, 2007.
25 R. H. M. Vandeleur, *Polymer*, 1994, **35**, 2691–2700.
26 B. A. Bedekar, Y. Tsujii, N. Ide, Y. Kita, T. Fukuda and T. Miyamoto, *Polymer*, 1995, **36**, 4735–4740.
27 T. Sato, Y. Tsujii, Y. Kita, T. Fukuda and T. Miyamoto, *Macromolecules*, 1991, **24**, 4691–4697.
28 S. Tasaka, N. Inagaki, S. Miyata and T. Chiba, *Sen'i Gakkaishi*, 1988, **44**, 546–550.
29 J. Y. Kim, H. Kim, T. Kim, S. Yu, J. W. Suk, T. Jeong, S. Song, M. J. Bae, I. Han, D. Jung and S. H. Park, *J. Mater. Chem. C*, 2013, **1**, 5078–5083.
30 T. Zhang, M. H. Litt and C. E. Rogers, *J. Polym. Sci., Part A: Polym. Chem.*, 1994, **32**, 2809–2816.
31 T. Zhang, M. H. Litt and C. E. Rogers, *J. Polym. Sci., Part A: Polym. Chem.*, 1994, **32**, 2291–2300.
32 J. Wei, Z. Zhang, J.-K. Tseng, I. Treufeld, X. Liu, M. H. Litt and L. Zhu, *ACS Appl. Mater. Interfaces*, 2015, **7**, 5248–5257.
33 Y. X. Wang, X. Y. Huang, T. Li, Z. W. Wang, L. Q. Li, X. J. Guo and P. K. Jiang, *J. Mater. Chem. A*, 2017, **5**, 20737–20746.
34 Y.-F. Zhu, Z. Zhang, M. H. Litt and L. Zhu, *Macromolecules*, 2018, **51**, 6257–6266.
35 Z. Zhang, D. H. Wang, M. H. Litt, L.-S. Tan and L. Zhu, *Angew. Chem., Int. Ed.*, 2018, **57**, 1528–1531.
36 N. Du, G. P. Robertson, I. Pinnau and M. D. Guiver, *Macromolecules*, 2009, **42**, 6023–6030.
37 Z. Zhang, M. H. Litt and L. Zhu, *Macromolecules*, 2018, **51**, 1967–1977.
38 S. Wu, W. Li, M. Lin, Q. Burlingame, Q. Chen, A. Payzant, K. Xiao and Q. M. Zhang, *Adv. Mater.*, 2013, **25**, 1734–1738.
39 Q. Li, L. Chen, M. R. Gadinski, S. Zhang, G. Zhang, H. U. Li, E. Iagodkine, A. Haque, L.-Q. Chen, T. N. Jackson and Q. Wang, *Nature*, 2015, **523**, 576–579.

 This journal is © The Royal Society of Chemistry 2020

40 S. Sucharitakul, N. J. Goble, U. R. Kumar, R. Sankar, Z. A. Bogorad, F. C. Chou, Y. T. Chen and X. P. A. Gao, *Nano Lett.*, 2015, **15**, 3815–3819.
41 K. Premasiri, S. K. Radha, S. Sucharitakul, U. R. Kumar, R. Sankar, F. C. Chou, Y. T. Chen and X. P. A. Gao, *Nano Lett.*, 2018, **18**, 4403–4408.
42 D. A. Bandurin, A. V. Tyurnina, G. L. Yu, A. Mishchenko, V. Zólyomi, S. V. Morozov, R. K. Kumar, R. V. Gorbachev, Z. R. Kudrynskyi, S. Pezzini, Z. D. Kovalyuk, U. Zeitler, K. S. Novoselov, A. Patanè, L. Eaves, I. V. Grigorieva, V. I. Falko, A. K. Geim and Y. Cao, *Nat. Nanotechnol.*, 2016, **12**, 223–227.
43 H. Wang, Y. Wu, C. Cong, J. Shang and T. Yu, *ACS Nano*, 2010, **12**, 7221–7228.
44 W. Feng, W. Zheng, W. Cao and P. Hu, *Adv. Mater.*, 2014, **26**, 6587–6593.

Published on 31 octubre 2019. Downloaded on 31/7/2024 01:20:01.